Thermal behaviour of multilayer and functionally-graded YSZ /$Gd_2Zr_2O_7$ coatings

P. Carpio[a*], M.D. Salvador[a], A. Borrell[a], E. Sánchez[b]

▪ Instituto de Tecnología de Materiales (ITM), Universitat Politècnica de València (UVP). Camino de Vera s/n, 46022 Valencia, Spain

• Instituto de Tecnología Cerámica (ITC), Universitat Jaume I (UJI). Campus Universitario Riu Sec, Av. Sos Baynat s/n, 12006 Castellón, Spain

[*] Corresponding autor: Pablo Carpio

Telephone number: 0034 963870000 ext:19625

E-mail address: pabcarco@upv.es

Complete postal address: Ciudad Politécnica de la Innovación, Semisótano Ed. 8B, Camino de Vera s/n, 46022 Valencia, Spain

Abstract

Zirconates with pyrochlore structure, such as $Gd_2Zr_2O_7$, are new promising thermal barrier coatings because of their very low thermal conductivity and good chemical resistance against molten salts. However, their coefficient of thermal expansion is low, therefore their thermal fatigue resistance is compromised. As a solution, the combination of yttria-stabilised zirconia (YSZ) and $Gd_2Zr_2O_7$ can reduce the thermal contraction mismatch between the thermal barrier coating parts.

In the present study, two possible designs have been performed to combine YSZ/ $Gd_2Zr_2O_7$. On the one hand, a multilayer coating was obtained where YSZ layer was deposited between a $Gd_2Zr_2O_7$ layer and a bond coat. On the other hand, a functionally-graded coating was designed where different layers with variable ratios of YSZ/$Gd_2Zr_2O_7$ were deposited such that the composition gradually changed along the coating thickness.

Multilayer and functionally-graded coatings underwent isothermal and thermally-cycled treatments in order to evaluate the oxidation, sintering effects and thermal fatigue resistance of the coatings. The YSZ/$Gd_2Zr_2O_7$ multilayer coating displayed better thermal behaviour than the $Gd_2Zr_2O_7$ monolayer coating but quite less thermal fatigue resistance compared to the conventional YSZ coating. However, the functionally-graded coating displays a good thermal fatigue resistance. Hence, it can be concluded that this kind of design is ideal to optimise the behaviour of thermal barrier coatings.

Keywords: E. Thermal applications; C. Thermal properties; D. ZrO_2 and earth-rare zirconates; B; Multilayers and functionally-graded coatings

1. **Introduction**

Thermal barrier coatings (TBCs) are commonly used to protect the metallic parts of gas turbines against very hot environments. They are formed by different layers with different functions: a metallic substrate, an intermetallic bond coat and a ceramic top layer. Besides, a thermally-grown oxide (TGO) layer of Al_2O_3 appears between the bond coat and the ceramic layer during the TBC lifespan due to a selective oxidation of the bond coat [1, 2]. One of the most used techniques to obtain the TBC is the atmospheric plasma spraying (APS) owing to its easy industrial-scaling, in addition to the resultant coating microstructure that brings on a thermal conductivity reduction [3, 4].

The most common material used as ceramic layer is the yttria-stabilised zirconia (YSZ) because of their low thermal conductivity and good mechanical behaviour at high temperature. However, YSZ displays a crystalline-phase change at long lifetimes or at very high temperatures (> 1200 ºC) which causes a damage or failure of the TBC. Different alternative materials to YSZ have been studied in order to develop TBCs for higher temperature applications. One of the most promising materials is the zirconate with pyrochlore structure [5-7] because of its significantly low thermal conductivity and a high phase stability. $Gd_2Zr_2O_7$ is the zirconate that displays the best resistance against the molten salt attack. However, the low coefficient of thermal expansion (CTE) of the zirconates in general, and $Gd_2Zr_2O_7$ in particular, make it impossible to use this kind of materials on its own as a TBC ceramic layer [8, 9]. The CTE mismatch among the different layers that form the TBC is quite high (metallic and ceramic parts display a high and low CTE, respectively). Therefore, it is necessary that the ceramic layer possesses the highest possible CTE with the aim of reducing the stresses caused during thermal cycles, which the gas turbines experiment [8, 9].

One possible solution used by other authors consisted in designing a multilayer coating where a YSZ layer is deposited between the bond coat and the $Gd_2Zr_2O_7$ layer so that the CTE between the coatings is reduced [8, 10]. The previous works present a multilayer design optimising the properties of both ceramics, although adherence problems between coatings can appear due to a pronounced change of properties inside the coating [10]. A second possibility that avoids this problem consists in gradually changing the composition along the coating thickness. This design is known as functionally-graded materials (FGM) and it is achieved depositing layers with different compositional ratios [11, 12].

In the present work, YSZ and $Gd_2Zr_2O_7$ monolayers as well as YSZ/$Gd_2Zr_2O_7$ multilayer and functionally-graded coatings were obtained by APS. The coatings underwent isothermal and thermally-cycled treatments at different times or thermal cycles, to evaluate their behaviour during the typical gas turbine life. The evolution of coating microstructure (porosity and cracks), as well as the mechanical properties, were recorded with the aim of evaluating the sintering and thermal fatigue effects. Besides, the growth of the TGO layer was also recorder to evaluate the oxidation resistance of

the bond coat and its influence on the coating damage. From these results, differences on the degradation mechanism between isothermal and thermally-cycled treatments were assessed. Moreover, the resistance against thermal treatments was compared among the obtained coatings in order to find improvements in multilayer and functionally-graded coatings.

2. Experimentation

2.1. Coating manufacturing

Two commercial feedstock powders were used as raw material for TBCs ceramic layers: YSZ (Metco 204-NS, Oerlikon-Metco, Germany) and $Gd_2Zr_2O_7$ (Amperit® 835.006, H.C. Starck, Germany). The main powder characteristics are shown in Table 1. The crystalline phases in these feedstocks were identified by X-ray diffraction (D8 Advance, Bruker AXS, Germany). In addition, a scanning electron microscopy (JSM 6300, JEOL, Japan) linked to an electron-dispersive X-ray spectroscopy detector (EDX) was used to analyse the feedstock microstructure and composition. Finally, granule apparent specific mass was calculated from powder tapped specific mass, assuming a theoretical packing factor of 0.6, which is characteristic of monosized, spherical particles [13].

The TBCs obtained is formed by a substrate, a bond coat and a ceramic layer. The substrate was a nickel-based superalloy (Inconel 718), which is ideal for high temperature applications. A bond coat (AMDRY 997, Oerlikon-Metco, Germany) was used to enhance the adhesion between the substrate and the ceramic layers. Besides, it plays an important role in the oxidation resistance [1]. Bond coat composition was Ni-23Co-20Cr-9Al-4.2Ta-0.6Y. The bond coat and, then, the ceramic layers were deposited onto the substrate by an atmospheric plasma spray (APS) system. The system consisted of a mono-cathode plasma gun (F4-MB, Oerlikon-Metco, Germany) operated by a 6-axis robot (IRB 1400, ABB, Switzerland). Before spraying, the substrate was grit-blasted with corundum at a pressure of 4.2 bars and cleaned with ethanol to remove any remaining dust or grease from the surface. YSZ and $Gd_2Zr_2O_7$ powders were sprayed to develop the ceramic layer using the same spraying parameters. Table 2 shows the spraying parameters of bond coat and ceramic layers.

Four different coatings were studied in which the ceramic layer configuration was modified. On one hand, YSZ and $Gd_2Zr_2O_7$ monolayer coatings were prepared depositing the corresponding feedstock (15 spraying passes) onto the bond coat. Then, multilayer coating was developed applying 5 spraying passes of YSZ powder and then 10 spraying passes of $Gd_2Zr_2O_7$. The ratio between the thicknesses of different layers was taken from preliminary studies [8]. Finally, functionally-graded coatings were obtained depositing various layers of 2 spraying passes/layer with different YSZ/$Gd_2Zr_2O_7$ ratios: 100% YSZ powder onto bond coat; 75% YSZ/25% $Gd_2Zr_2O_7$; 50% YSZ/50% $Gd_2Zr_2O_7$; 25% YSZ/75 $Gd_2Zr_2O_7$; and 100% $Gd_2Zr_2O_7$ (% in mass). More details about the system employed to obtain multilayer and functionally-graded

coatings can be consulted elsewhere [14, 15]. Fig. 1 schematically illustrates the design of the four studied coatings. All coatings were designed so that their thicknesses were approximately 200 μm.

It is important to note that the multilayer and the functionally-graded coatings were acquired using two independent feed systems (one for each powder) with their respective circuits. The two powders were thus injected into the plasma plume via two different nozzles arranged radially around the torch. This procedure differs from other works where the grades had been carried out mixing the powders prior to the spraying process. This supposes an easier production because it is unnecessary to get as many compositions as desirable grades [16, 17].

2.2. Isothermal and thermally-cycled treatments

Isothermal and thermally-cycled treatments were carried out with a vertical tubular furnace (Energon SL, Spain) to evaluate the coating behaviour against the sintering, oxidation and thermal fatigue effects. The cycling tests were performed with the aid of a vertical elevator, which enables that the samples quickly change from the heating stage inside the furnace to the cooling stage using a forced airflow outside the furnace.

In the case of thermally-cycled treatments, the samples underwent several thermal cycles up to detachment of the coating. The number of cycles that the coating was kept without being detached was considered as the reference of the thermal fatigue resistance value. For this purpose, a visual examination was performed after every 50 cycles. The thermal cycles consisted on 600-s soaking time at 1050 ºC and 300-s forced air-cooling at room temperature. Furthermore, isothermal treatments were performed at the same temperature (1050 ºC) to compare thermal degradation phenomena in both treatments; the soaking time varied (20, 50 and 100 h) and the cooling was slow to avoid damages originated by thermal fatigue.

2.3. Microstructural and mechanical characterisation

Coatings were microstructurally and mechanically characterised as-sprayed as well as at different after thermal-cycle tests and soaking times (isothermal test).

Micrographic examination and microprobe analysis were performed by means of scanning electron microscopy (SEM) with an X-ray detector (EDX). The sample cross-sections were prepared by metallography prior to the micrographic examination by means of mounting inside a two-phase epoxy resin and polishing up to an abrasive step of 0.25 μm. Porosity and crack areas were quantified from SEM backscattering electron micrographs using image analysis software (Image-Pro Plus). Besides, TGO layer was detected by element compositional mapping and, then, its thickness was measured from SEM micrographs. On the other hand, the crystalline phases were identified by X-ray diffraction (XRD).

Vickers microhardness was measured with a microhardness tester (HMV-2, Shimadzu, Japan), performing 10 indentations at 200 g for 10 s. Two indentations at different thicknesses (50 and 150 μm) were performed to determine the microhardness variation along the coating and to relate this variation to the compositional changes.

3. Results and discussion

3.1. As-sprayed coatings

Microstructure of as-sprayed YSZ and $Gd_2Zr_2O_7$ monolayers as well as multilayer and functionally-graded coatings can be observed in Fig. 2. All microstructures display the substrate in the bottom, the bond coat in the middle and ceramic layer on top. The TGO layer cannot be seen because it is formed during thermal treatments. The different layers exhibited the typical APS microstructure formed by splats with a longitudinal orientation. Some cracks in the splat borders and porosity were retained between the splats. Few vertical cracks were also observed, attributing this behaviour to the fast cooling of the molten splat [3, 4]. The YSZ monolayer coating exhibited a similar porosity as that of $Gd_2Zr_2O_7$ when using the same plasma spraying parameters (Fig. 2a and b) because the higher thermal conductivity of YSZ is counteracted with its higher melting temperature [18].

In the case of multilayer coating (Fig. 2c), two ceramic layers were clearly identified, being $Gd_2Zr_2O_7$ the light layer on the top while YSZ corresponds to the darker layer situated between $Gd_2Zr_2O_7$ layer and bond coat. Finally, functionally-graded coatings (Fig. 2d) were formed by dark and light splats, which correspond to YSZ and $Gd_2Zr_2O_7$, respectively. The ratio of YSZ/$Gd_2Zr_2O_7$ splats changed along the thickness so that the top part was formed only by $Gd_2Zr_2O_7$ while the part closer to the bond coat was composed only by YSZ. The coating elemental composition was 40 wt% ZrO_2 / 60 wt% Gd_2O_3 the composition of light zones and 93 wt% ZrO_2 / 7 wt% Y_2O_3 in dark zones. No Gd_2O_3 was found in dark zones, therefore no chemical interaction was produced between YSZ and $Gd_2Zr_2O_7$.

Fig. 3 displays the diffractogram patterns of as-sprayed YSZ and $Gd_2Zr_2O_7$ coatings, being tetragonal ZrO_2 and the $Gd_2Zr_2O_7$ with pyrochlore structure, respectively, the only identified phases. The 50% YSZ and 50% $Gd_2Zr_2O_7$ coating exhibited the same crystalline phases that coatings from both compositions deposited separately, what corroborates no chemical interaction among the feedstocks during the deposition. No changes in the crystalline-phases were found after isothermal treatment at 100 h soaking-time, confirming the thermal stability of the phases.

It is important to note that it was possible to deposit the $Gd_2Zr_2O_7$ monolayer coating by APS. However, this coating easily spalled when any thermal treatment was applied. For this reason, the $Gd_2Zr_2O_7$ monolayer coating is omitted in the following discussions.

3.2. Isothermal treatment

Fig. 4 shows the cross-section microstructures of coatings isothermally-treated at 100 h soaking time. The most important microstructural change between as-sprayed and isothermally-treated coatings was the formation of a TGO layer between the bond coat and the ceramic layer (it is marked in Fig. 4). The composition of the TGO layer was Al_2O_3, corroborated by element mappings. Oxidation of bond coat occurs due to the diffusion of atmospheric oxygen through the porous ceramic layers. The mechanism of diffusion through the top consists on: (i) ionic movement of oxygen, and (ii) oxygen ingress through interconnected pores and cracks. In Fig. 5, it is observed that the kinetics of TGO formation is faster at shorter times due to Al availability and the low free energy of Al_2O_3 formation. However, the kinetics progressively slows down because Al_2O_3 acts as a diffusion barrier, offering resistance to further oxygen diffusion and approaching steady state [17]. According to previous studies, the TGO growth kinetics can be expressed through the following equation [17, 19]:

$$h^n = k_p \cdot t \quad (1)$$

where h is the TGO thickness (m), t is the thermal treatment time (s), k_p is the rate constant ($m^2 \cdot s^{-1}$), and n is taken as 2 when the growth mechanism is assumed to be diffusion assisted. The TGO formation of the studied coatings were fitted adequately to equation 1, where the corresponding rate constant and correlation coefficient are shown in Table 3. The rate constants were similar to those of YSZ coatings reported in previous works [19]. However, the multilayer rate constant is slightly lower probably because $Gd_2Zr_2O_2$ layer acts as a more effective oxygen diffusion barrier than YSZ.

Evolution of porosity, cracks, and hardness is also presented in Fig. 5. The porosity was reduced during the first 20 h of isothermal treatment and then porosity remained practically invariable at longer times. This reduction was caused by the sintering effect, where material diffusion to the voids occurs. The sintering also provoked the formation of sintering necks between cracks along areas where material had diffused. The formation of sintering necks causes a closing of the cracks, as a consequence, the smooth and straight cracks were separated into smaller parts and a reduction of crack ratio was determined, as reflected in Fig. 5 [20]. The reduction of porosity and cracks in the coatings caused hardening so that the coating hardness rises during the first 20 h of thermal treatment. Another effect of the sintering was the coalecence of pores so that coarser and rounded voids were formed at higher soak times. In fact, a rise of the porosity was observed because it was measured by image analysis and very fine pores were hardly identified by this technique. However, previous works, where the porosity was measured by mercury porosimetry, revealed that porosity was reduced at high soak times but the mean void size was increased [20]. Other authors noted that a cracking during isothermal treatment is formed due to the TGO thickening that promotes out of plane stresses at the TGO and ceramic layer interfaces [21]. Nevertheless, this cracking was not observed in the present case because TGO thickening was slow and, hence, the cracking effect was counteracted by the sintering effect.

3.3. Thermally cycled treatment

Fig. 6 plots thermal fatigue resistance. As expected monolayer $Gd_2Zr_2O_2$ coating was unsuitable as TBC material because it cannot withstand the thermal fatigue. On the other hand, the YSZ monolayer coating exhibited a very high thermal fatigue resistance because of high toughness and coefficient of thermal expansion. Regarding multilayer and functionally-graded coatings, their resistances resulted between those of YSZ and $Gd_2Zr_2O_2$ monolayer coatings, although differences among them were observed. The functionally-graded coating produced a higher resistance to the thermal cycles than that of the multilayer coating because the composition was gradually-changed along the thickness; therefore the stress generated was homogenously distributed. These results are explained by the different microstructural evolution of the coatings, which can be observed in Fig. 7 and Fig. 8.

During the first thermal cycles the porosity was reduced due to sintering effect, just as it occurred during the isothermal treatment. However, thermal stresses inside the ceramic layers were generated; hence the formation of microcracks between the already sprayed layers and freshly sprayed splats was observed [22]. In the case of functionally-graded coatings, the microcrack formation was more pronounced since splats with different CTE were distributed along the whole ceramic layer. Regarding the coating microhardness, this property was increased even more than in isothermal treated coatings. Therefore, this cannot be only attributed to the sintering effect but to the thermal stresses that inhibit plastic deformation.

At higher thermal-cycles, the stresses caused by the difference in CTE between layers were too important and the microcracks were connected. This connection gave rise to horizonal (longitudinal) macrocrack propagation. The macrocracks were formed inside YSZ layer close to the bond coat interface because the greatest thermal expansion mismatch occurred between those layers. Finally, the ceramic layers detached when the macrocrack formation was too critical, as it can be observed in Fig. 9. Vertical (transversal) cracks were also formed during the thermal cycles, as it can be observed at Fig. 7. The appearance of this kind of cracks is due to the gradient of temperature inside the coatings, which is originated during the temperature changes [23]. Regarding the porosity, the cracks were detected as pores by the image analysis software; therefore, a slight porosity increment can also be observed in Fig. 8. Despite the fact that the failure mechanism was similar in the three coatings, the presence of horizontal and vertical macrocraks occurred at a different number of thermal cycles, what is related with the thermal fatigue resistance of each coating. The thermal stresses were more concentrated in the YSZ layer of multilayer coatings because this layer was placed between the other two layers (bond coat and $Gd_2Zr_2O_2$ layers) with different CTE. Consequently, macrocraking propagation occurred immediately after microcraking formation at approximately 500 cycles (Fig. 7-b). However, macrocraking formation and coating detachment was slowed down in the YSZ monolayer and functionally-graded coatings because the thermal stress were more evenly distributed in the whole ceramic layer (Fig.

7-d and e). Coating damage caused by the macrocraking formation leads to a slight worsening of mechanical properties in addition to the reduction of the coating lifetime.

A TGO layer was also formed during thermal-cycles in the same manner as during isothermal treatment. Their kinetics was also fitted with a parabolic law (equation 1) and the fit adjustment parameters are shown in Table 3. For the fit, only the heating time was considered (600 s per cycle), taking into account that this is an approximation because the whole sample took some time to reach the maximum temperature. The TGO thickening mechanism was practically invariable in thermally-cycled and isothermal treatments since rate constants were similar in spite of the approximation cited above. Hence, the formation and propagation of cracks during cycled treatments cannot be attributed to the TGO growth. TGO kinetics was slightly faster in the functionally-graded coating because the microcrack formation and, consequently, the oxygen diffusion were higher.

4. Conclusions

Multilayer and functionally-graded YSZ/$Gd_2Zr_2O_7$ coatings were successfully developed by APS using simultaneously two independent feed systems. Coatings displayed the desired structure and the only present crystalline phases were tetragonal ZrO_2 and pyrochlore-type $Gd_2Zr_2O_7$.

Then, these coatings underwent different thermal treatments with the aim of evaluating their sinterability and thermal fatigue resistance. The sintering effect was effective at short times of thermal treatments and this effect caused porosity and crack reduction, which results in a coating hardening effect. Regarding the thermal fatigue resistance, the coating detachment occurred at a specific number or thermal-cycles because thermal stresses were created due to the difference of CTE between layers. These thermal stresses initiated microcracking, shown as beneficial for mechanical properties. However, crack coalescence produced macrocracking responsible for coating detachment. Finally, the TGO layer grew after the thermal treatments similarly in isothermal and cycled treatments. TGO thickening was quite slow; therefore, it hardly caused stresses in adjacent layers.

Although the damage mechanisms are similar in all coatings, significant differences were observed among them. $Gd_2Zr_2O_7$ must be used combined with YSZ because its CTE is too low so that this layer was detached from the bond coat. Two possible combinations dealt with the multilayer and functionally-graded design. In both cases, the thermal fatigue resistance was lower than that of the conventional YSZ coating, although functionally-graded coatings exhibited less resistance difference. This can be explained by the distribution of splats with different compositions along the whole coating, allowing a homogeneous distribution of the thermal stresses and the microcrack formation, which slowed down the microcracks coalescence and the formation of longitudinal macrocracks. In conclusion, functionally-graded YSZ/$Gd_2Zr_2O_7$ coatings represent an ideal design for TBCs that takes advantage of the innovative properties (a

very low thermal conductivity as well as good chemical resistance) of $Gd_2Zr_2O_7$ with thermal fatigue resistance being hardly affected.

Acknowledgement

This work has been supported by the Spanish Ministry of Economy and Competitiveness (project MAT2015-67586-C3-R). A. Borrell acknowledges the Spanish Ministry of Economy and Competitiveness for her Juan de la Cierva-Incorporación contract (IJCI-2014-49839) and the Program to Support Research and Development (PAID-00-15) of the Universitat Politècnica de València. P. Carpio acknowledges the Valencia Government for his post-doc contract (APOSTD/2016/040).

Reference

[1] D.R. Clarke, M. Oechsner, N.P. Padture, Thermal-barrier coatings for more efficient gas-turbine engines, MRS Bull. 37 (2012) 891–898.

[2] C.U. Hardwicke, Y.C. Lau, Advances in thermal spray coatings for gas turbines and energy generation: A review, J. Therm. Spray Technol. 22 (2013) 564–576.

[3] S. Sampath, U. Schulz, M.O. Jarligo, S. Kuroda, Processing science of advanced thermal-barrier systems, MRS Bull. 37 (2012) 903–910.

[4] P. Fauchais, Understanding plasma spraying, J. Phys. D. Appl. Phys. 37 (2004) R86–R108.

[5] R. Vassen, A. Stuke, D. Stöver, Recent developments in the field of thermal barrier coatings, J. Therm. Spray Technol., 2009: pp. 181–186.

[6] G. Moskal, Criteria of assessment of powders provided to spray by the APS method for new and conventional layers type TBC, Arch. Mater. Sci. Eng. 37 (2009) 29–36.

[7] Z.H. Xu, X. Zhou, K. Wang, J.W. Dai, L.M. He, Thermal barrier coatings of new rare-earth composite oxide by EB-PVD, J. Alloys Compd. 587 (2014) 126–132.

[8] E. Bakan, D.E. Mack, G. Mauer, R. Va??en, Gadolinium zirconate/YSZ thermal barrier coatings: Plasma spraying, microstructure, and thermal cycling behavior, J. Am. Ceram. Soc. 97 (2014) 4045–4051.

[9] J.M. Drexler, C.H. Chen, A.D. Gledhill, K. Shinoda, S. Sampath, N.P. Padture, Plasma sprayed gadolinium zirconate thermal barrier coatings that are resistant to damage by molten Ca-Mg-Al-silicate glass, Surf. Coatings Technol. 206 (2012) 3911–3916.

[10] X. Zhong, H. Zhao, X. Zhou, C. Liu, L. Wang, F. Shao, K. Yang, S. Tao, C. Ding, Thermal shock behavior of toughened gadolinium zirconate/YSZ double-ceramic-layered thermal barrier coating, J. Alloys Compd. 593 (2014) 50–55.

[11] X. Chen, L. Gu, B. Zou, Y. Wang, X. Cao, New functionally graded thermal barrier coating system based on $LaMgAl_{11}O_{19}$/YSZ prepared by air plasma spraying, Surf. Coatings Technol. 206 (2012) 2265–2274

[12] S. Zhao, Y. Zhao, B. Zou, X. Fan, J. Xu, Y. Hui, X. Zhou, S. Liu, X. Cao, Characterization and thermal cycling behavior of $La2(Zr_{0.7}Ce_{0.3})_2O_7$/8YSZ functionally graded thermal barrier coating prepared by atmospheric plasma spraying, J. Alloys Compd. 592 (2014) 109–114.

[13] J.L.A. Albaro, a B. Fuentes, J.E.E. Navarro, F.N. Medall, Características de polvos cerámicos para prensado, Bol. Soc. Esp. Ceram. Vidr. 26 (1987) 31–37.

[14] P. Carpio, E. Bannier, M.D. Salvador, R. Benavente, E. Sánchez, Multilayer and particle size-graded YSZ coatings obtained by plasma spraying of micro- and nanostructured feedstocks, J. Therm. Spray Technol. 23 (2014) 1362–1372.

[15] P. Carpio, E. Rayón, M.D. Salvador, L. Lusvarghi, E. Sánchez, Mechanical Properties of couble-Layer and graded composite coatings of YSZ obtained by atmospheric plasma spraying, J. Therm. Spray Technol. 25 (2016) 778–787.

[16] V. Petrova, S. Schmauder, FGM/homogeneous bimaterials with systems of cracks under thermo-mechanical loading: Analysis by fracture criteria, Eng. Fract. Mech. 130

(2014) 12–20.

[17] S. Nath, I. Manna, J.D. Majumdar, Kinetics and mechanism of isothermal oxidation of compositionally graded yttria stabilized zirconia (YSZ) based thermal barrier coating, Corros. Sci. 88 (2014) 10–22.

[18] X.Q. Cao, R. Vassen, D. Stoever, Ceramic materials for thermal barrier coatings, J. Eur. Ceram. Soc. 24 (2004) 1–10.

[19] M. Madhwal, E.H. Jordan, M. Gell, Failure mechanisms of dense vertically-cracked thermal barrier coatings, Mater. Sci. Eng. A. 384 (2004) 151–161.

[20] B. Siebert, C. Funke, R. Vaben, D. Stöver, Changes in porosity and Young's Modulus due to sintering of plasma sprayed thermal barrier coatings, J. Mater. Process. Technol. 92-93 (1999) 217–223.

[21] A. Rico, J. Gómez-García, C.J. Múnez, P. Poza, V. Utrilla, Mechanical properties of thermal barrier coatings after isothermal oxidation. Depth sensing indentation analysis, Surf. Coatings Technol. 203 (2009) 2307–2314.

[22] J. Sure, K. Thyagarajan, C. Mallika, U.K. Mudali, Thermal-Cycling Behavior of Plasma-Sprayed Partially Stabilized Zirconia Coatings on High-Density Graphite Substrate, J. Therm. Spray Technol. 24 (2015) 925–937.

[23] H.B. Guo, R. Vaßen, D. Sto, Thermophysical properties and thermal cycling behavior of plasma sprayed thick thermal barrier coatings, Surf. Coatings Technol. 192 (2005) 48 – 56.

Table list

Table 1. Characteristics of the feedstocks

	YSZ	**$Gd_2Zr_2O_7$**
Chemical composition (wt%)	ZrO_2: 92 Y_2O_3: 8	ZrO_2: 40 Gd_2O_3: 60
Main crystalline phases	Tetragonal ZrO_2	Pyrochlore type - $Gd_2Zr_2O_7$
Granule specific weight (kg/m^3)	4500	3600
Average granule size (μm)	55	82

Table 2. Main plasma spraying parameters of each layer

	Bond coat	**Ceramic layer**
Ar flow rate (slpm*)	65	35
H_2 flow rate (slpm*)	8	12
Intensity (A)	650	600
Spraying distance (m)	0.145	0.1
Spraying speed (m/s)	1	1
Feedstock flow rate (g/min)	**40**	**45**

*slpm: standard litre per minute

Table 3. TGO rate constant (k_p) and its corresponding correlation coefficient (R^2) of the samples isothermally and thermally-cycled treated

	Isothermal treatment		**Thermally-cycled treatment**	
	k_p (10^{-17}·m^2·s^{-1})	**R^2**	**k_p (10^{-17}· m^2·s^{-1})**	**R^2**
YSZ monolayer	1.68	0.98	1.38	0.99
YSZ/$Gd_2Zr_2O_2$ Multilayer	1.50	0.98	1.54	0.99
YSZ/$Gd_2Zr_2O_2$ **Functionally-graded**	1.69	0.98	2.46	0.98

Figure captions

Fig 1. Schematic illustration of the four coatings: a) monolayer YSZ; b) monolayer $Gd_2Zr_2O_7$; c) multilayer; d) functionally-graded

Fig. 2. Backscattering electron micrographs of as-sprayed coatings: a) monolayer YSZ; b) monolayer $Gd_2Zr_2O_7$; c) multilayer; d) functionally-graded

Fig. 3. XRD pattern of: a) YSZ coating; b) 50% YSZ + 50% $Gd_2Zr_2O_7$ coating; c) $Gd_2Zr_2O_7$ coating

Fig. 4. Backscattering electron micrographs of isothermally-treated coatings at 100 h soaking time: a) monolayer YSZ; b) multilayer; c) functionally-graded. t is refered to TGO layer

Fig. 5. Evolution of a) porosity, b) cracks, c) TGO thickness and d) microhardness at different soaking times

Fig. 6. Histogram of the thermal fatigue resistance of the different coatings

Fig. 7. Backscattering electron micrographs of thermally-cycled treated at a,b,c) 500 cycles and d,e) 1500 cycles of a,d) monolayer YSZ b) multilayer; c,e) functionally-graded. t, h and v are refered to TGO layer, horozontal macrocracks and vertical cracks, respectively

Fig. 8. Evolution of a) porosity, b) cracks, c) TGO thickness and d) microhardness at different thermal-cycles

Fig. 9. Backscattering electron micrograph multilayer coating at 950 thermal-cycles

Figure list

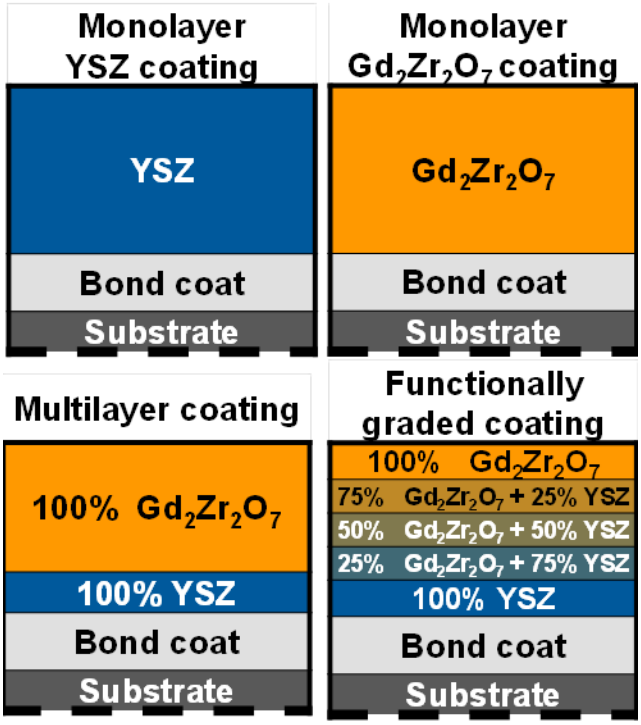

Figure 1

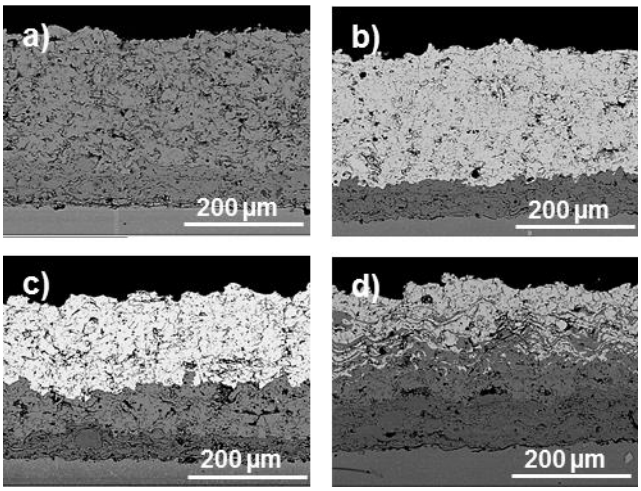

Figure 2

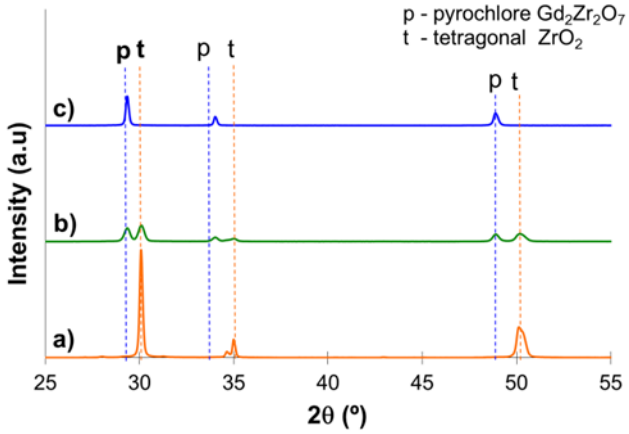

Figure 3

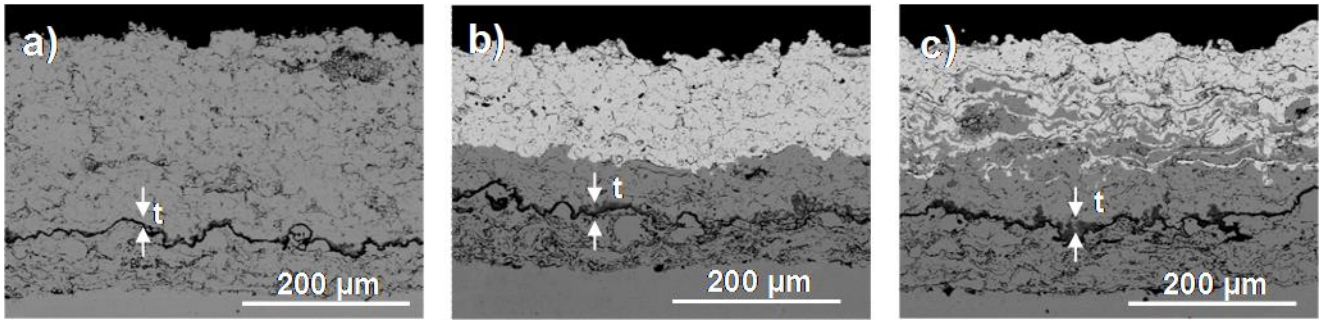

Figure 4

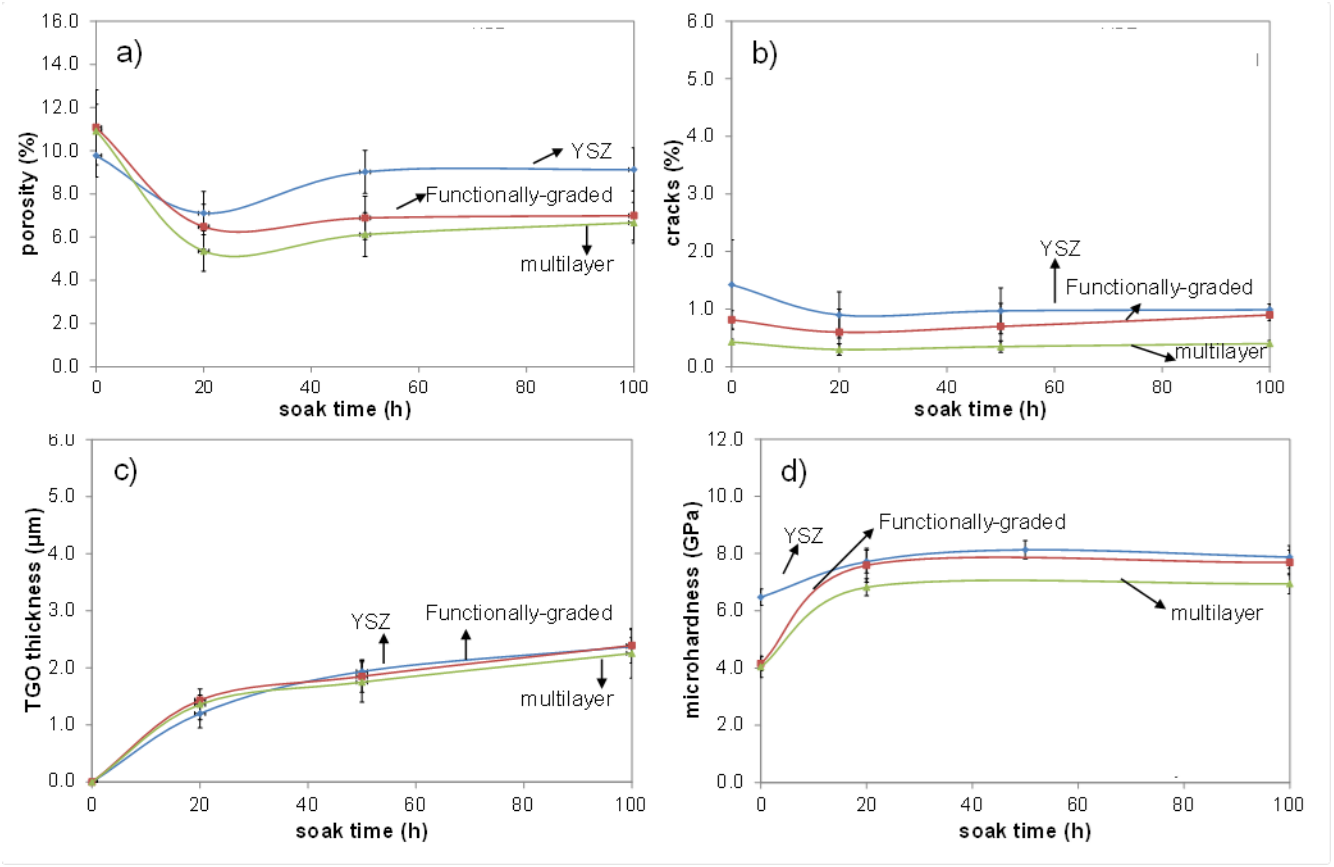

Figure 5

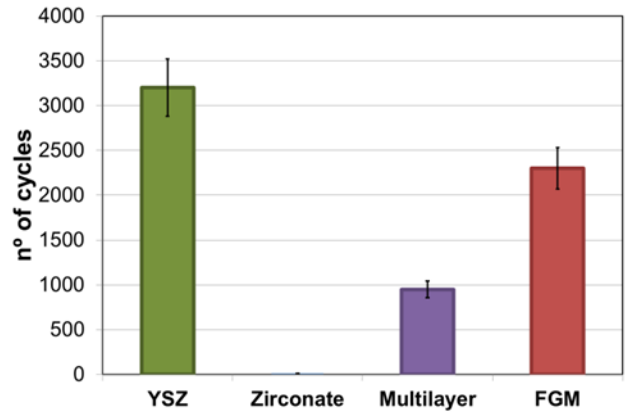

Figure 6

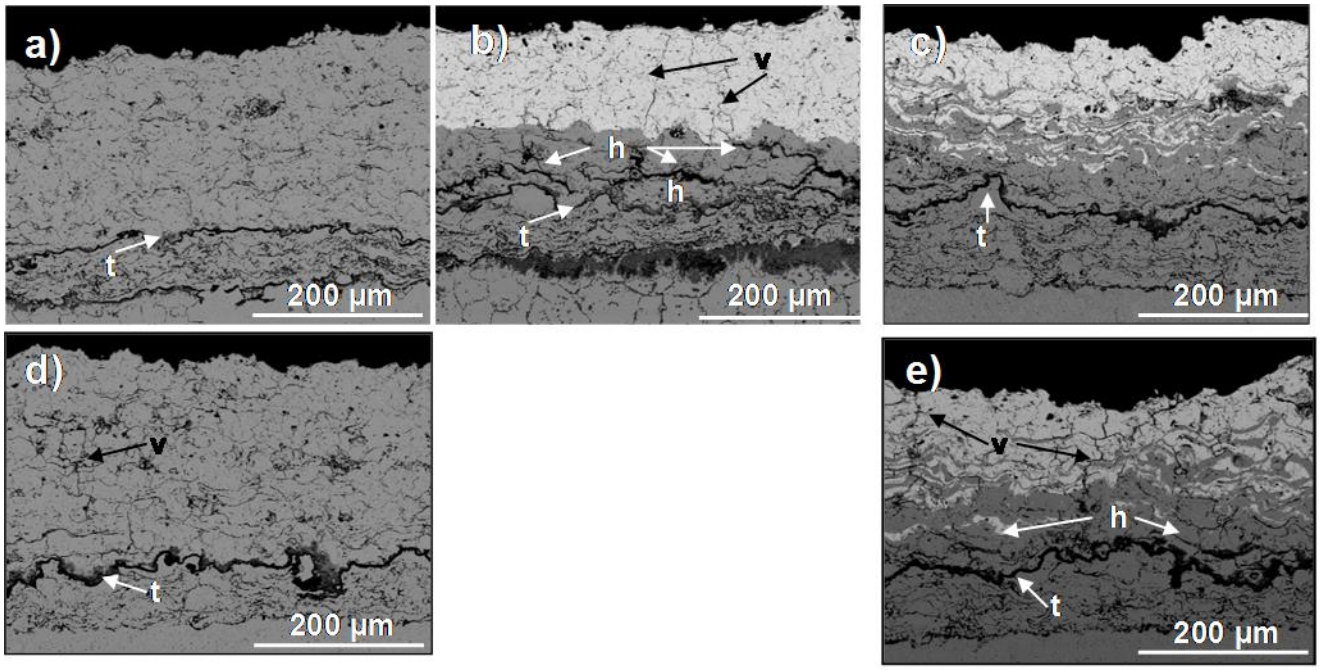

Figure 7

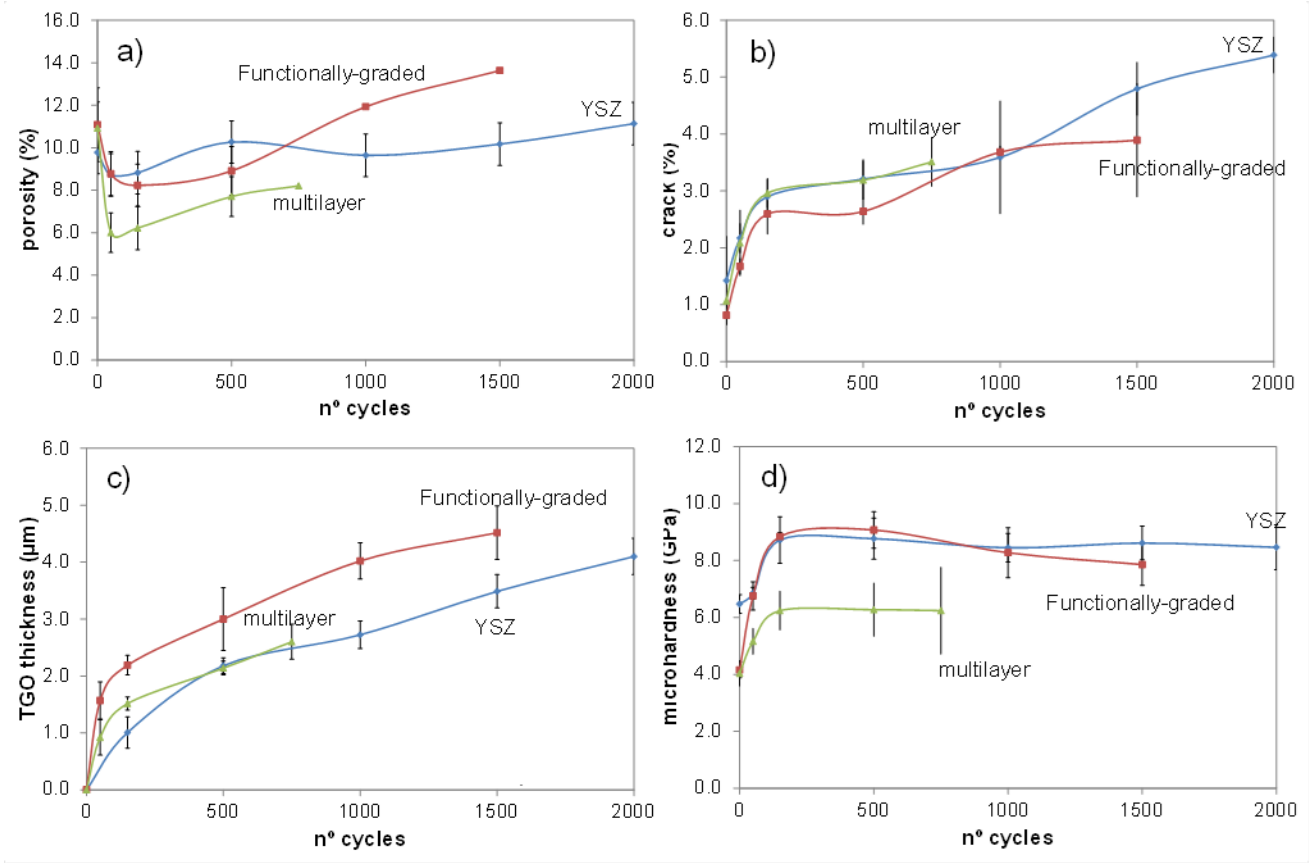

Figure 8

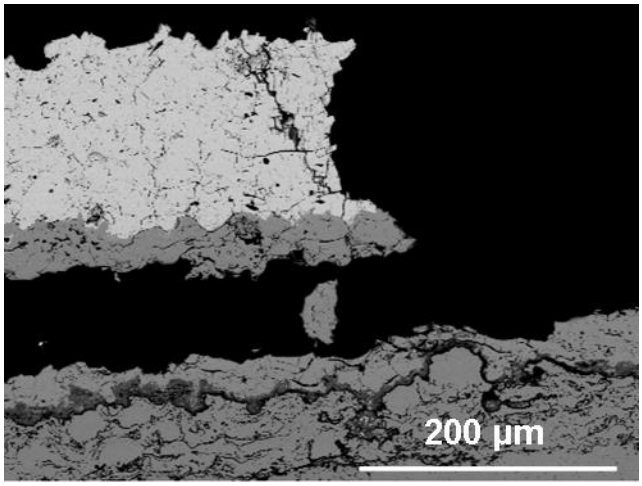

Figure 9